RESEARCH PAPER

Formation and Characterization of Zeolite Y-platinum Nanoparticles by Rapid Method of Ultrasonic Irradiation and Investigation of Its Electrochemical Property

Modarres Dehghani and Azadeh Tadjarodi *

Department of Chemistry, Iran University of Science and Technology, Narmak, Tehran, Iran

ARTICLE INFO

ABSTRACT

Zeolite has presented a unique crystalline structure with an excellent exchange capability formed by Al-O-Si, which it can be used as a good surface for dispersed metal particles. In this work, rapid synthesis of zeolite Y-platinum nanoparticles by ultrasonic treatment was studied. The structure and morphology of the prepared zeolite Y-platinum nanoparticles were characterized using X-ray diffraction (XRD), Fourier transform infrared spectroscopy (FT-IR), Scanning electron microscopy (SEM), Transmission electron microscopy (TEM), Energy-dispersive X-ray spectroscopy (EDS), Brunauer-Emmett Teller (BET), and EDS mapping analysis. In this work, we successfully developed a rapid and green method for the synthesis of zeolite Y and zeolite Y-platinum nanoparticles with uniform small crystals and high purities by the use of ultrasonic irradiations. The use of ultrasound irradiation has proved to be an environmentally sound, time and cost effective approach for various organic and inorganic compounds. Also, it is an excellent technique for the adherence of nanoparticles to a large variety of substrates. Investigation of the electrochemical characteristics of the prepared Z-Y-Pt NPs was carried out by the use of cyclic voltammetry (CV) test and it displays ratio of j_f/j_b=1.10 that can be suitable for redox reaction in fuel cell.

INTRODUCTION

Aluminosilicate zeolites are crystalline materials with a characteristic well-defined pore structures, strong acidity, and large surface area [1]. Si and Al are placed in the zeolite framework, as tetravalent and trivalent, respectively. Therefore, $SiO_{4/2}$ tetrahedral are electro-neutral, and $AlO_{4/2}$ tetrahedral are negatively charged [2]. Zeolites and related molecular sieves have gained great importance in many industrial applications. Some of the key applications of this materials are aromatization [3], isomerization [4], esterification [5], alkylation [6], cracking [7], methanol conversion [8] and selective oxidation [9]. Among them, zeolite Y (Z-Y) is one of the most important catalysts employed in isomerization, hydrocracking, and hydro-treating processes due to its three-dimensional pore structure with 12-membered ring channels [10-12].

The sound waves having frequencies above the audible range i.e. above 20 KHz are called ultrasonic waves. Generally these waves are called as high frequency waves [13]. Ultrasonic waves are known to cause the following effects in liquids: (1) activation of mass transport; (2) heating; (3) cavitation, i.e., generation of bubbles, which then collapse, giving rise to high local temperatures and pressures [14]. There are two types of sonochemical

* Corresponding Author Email: *tajarodi@iust.ac.ir*

reactions, homogenous sonochemistry that results from the formation of radicals or radical intermediates while heterogeneous sonochemistry is influenced primarily through the mechanical effects of cavitation, such as surface cleaning, particle size reduction, and improved mass transfer. Ultrasonic can accelerate chemical reactions by produce free radicals in solution. This leads to decomposition of oxygen and water molecules and generation of H and HO radicals: $H_2O \rightarrow {}^\bullet H + {}^\bullet OH$ [15]. These radicals can recombine to return to their original form or combine to produce H_2 and H_2O_2. These strong oxidants and reductants are utilized for various sonochemical reactions in aqueous solutions. Also, cavitations during of ultrasonic procedure cause chemical and physical phenomena due to ultrasonically driven growth and collapse of gas nuclei in a liquid. These cavitations are produced when gas nuclei that are present in the liquid go through oscillations expanding and compressing, during the expansion in ultrasonic field, a vacuum is created into which gas in the liquid diffuses. During the compression half of the cycle the gas within the bubble diffuses back into the host liquid, however, due to the smaller surface area not all the gas that diffused into the bubble diffuses out. After multiple expansion and compression, micro-bubbles reach a critical size resulting in bubble collapse during one compression cycle. Collapse of these bubbles results in adiabatic heating of gas and vapor inside the bubble. These cavitations produce radicals inducing sonochemical reactions. A simplified model of adiabatic bubble collapse can be used to calculate the maximum local temperature. These hot spots can reach a temperature of 5000 ºC, the local pressure can go as high as 20 MPa with high cooling rates of 107 ºC/s and this cavitation results in particle collisions at high velocities [15]. With a simple modification of reaction conditions, various forms of nanostructured materials can be synthesized. Ultrasonic energy can be used for the synthesis of metal and polymers, organic compounds, semiconductor particles, leather processing, drug delivery, cleaning of industrial equipment, interparticle collisions and coupled with electrochemical reactions [16-19]. Recently, the use of ultrasound in the synthesis of micrometer-sized (e.g. Na-A, Na-X, MCM-22) and nanometer-sized (e.g. Na-P, N-A, silicalite-1, SAPO-34) molecular sieves has been reported [20-24].

Nanoparticles are a special group of materials with a broad range of applications. They usually have a large surface area, which is chemically more reactive than their fine structural analogues. Metal nanoparticles have potential applications in various areas, such as cosmetics, electronics, packaging, coatings, and biotechnology [25-28]. Platinum is one of the rarest and expensive metals. It has high corrosion resistance and numerous catalytic applications including automotive catalytic converters and petrochemical cracking catalysts [29]. As one of the most promising alternative energies, fuel cells have been receiving increased attention recently due to the depletion of fossil fuels and the increase in environmental pollution. In order to enhance catalytic activity and to reduce the usage of Pt-based catalysts, one strategy is to explore novel carbon and zeolite materials as catalyst supports and to effectively disperse Pt-based particles on these supports.

Recently, we reported synthesis and characterization of zeolites Y-Pd NPs and Y-Pd-$NiFe_2O_4$ as suitable catalysts in Suzuki-Miyaura cross coupling reaction [30, 31]. In this work, the preparation and characterization of magnetic zeolite Y-platinum nanoparticles (Z-Y-Pt NPs) by ultrasonic treatment is reported. In this route, the crystallization temperature and synthesis time are shorter than in comparison other methods. In addition, Pt NPs have the average particle size of ~14 nm and they have uniform particulate morphology. The structure and morphology of the prepared Z-Y-Pt NPs were characterized using X-ray diffraction (XRD), Fourier transform infrared spectroscopy (FT-IR), Scanning electron microscopy (SEM), Transmission electron microscopy (TEM), Energy-dispersive X-ray spectroscopy (EDS), Brunauer-Emmett Teller (BET), and EDS mapping analysis. Also, the electrochemical features of the obtained Z-Y-Pt NPs was researched by cyclic voltammetry (CV).

MATERIALS AND METHODS

All of the compounds were purchased from Merck Company. Ultrasonic generation was carried out by an ultrasonic instrument (FAPA, Model: UP400) with a standard probe. SEM images and EDS were obtained by the use of ZEISS (Sigma VP-WDS detector) instrument. The powder X-ray diffraction was performed by a STOE-STADV instrument (Cu Kα = 1.5418 Å). FT-IR spectra were recorded with a Shimadzu spectrometer (KBr pellets) from 400 to 4000

cm^{-1}. TEM images were obtained using a Zeiss-EM10C-100 kV instrument. Brunauer Emmett Teller (BET) was obtained using a Micromeritics ASAP 2020 instrument.

Synthesis of Z-Y and H-Y

First, Z-Y was produced using a starting aluminosilicate gel with a molar ratio of 1 Al_2O_3/4 Na_2O/9 SiO_2/170 H_2O by ultrasonic method. Then, H-Y zeolite was obtained by ion exchange of Z-Y with a solution of ammonium chloride (1 M, 4 h, and reflux in 80 ºC), which we have reported in our previous paper [30].

Synthesis of Z-Y-Pt NPs using ultrasonic treatment

1 g of H-Y zeolite was added to 50 ml of ethanol in a 100 ml round-bottom flask and then H_2PtCl_6 (0.04 g) and KOH (0.45 g) were added to this solution. This mixture was dispersed by ultrasonic treatment for 1 h (150 W) at room temperature. After ultrasonic treatment, product was filtered, washed and was kept overnight at 120 ºC.

Electrochemical measurements

The electrochemical characteristics of the product was evaluated by CV test using a conventional three-electrode system in H2SO4 aqueous solution (0.5 M) on an electrochemical PG-State 204 workstation, Iran. The electrodes of Pt and saturated calomel were selected as the counter and reference electrodes, respectively. The scan rates of 0.05 Vs^{-1} with potential window of -0.4 to 1.0 V were considered to record CV curves.

RESULTS AND DISCUSSION

In this study, rapid synthesis of Z-Y and Z-Y-Pt NPs are reported. First, we considered three different times and different powers of ultrasonic instrument for the preparation of Z-Y. Our study shows that the best time for the synthesis of Z-Y is 3 h. Also, the most appropriate power for the synthesis is 150 W (Table 1). Fig. 1 shows XRD patterns of the prepared Z-Y in three different times (30, 120, and 180 min) with sharp diffraction
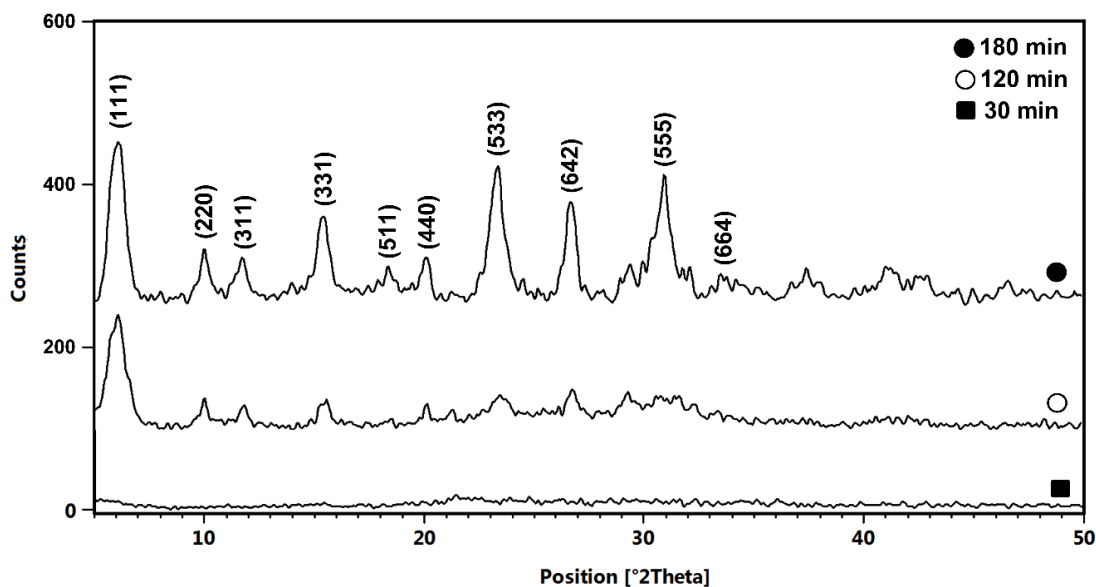

Fig. 1. XRD patterns for the formation of Z-Y in different times.

Table 1. Investigation different powers of ultrasonic instrument in the synthesis of Z-Y.

Entry	Condition (Ultrasonic irradiation, 3 h)	Product
1	50 W	Amorphous
2	100 W	Amorphous
3	150 W	Crystalline
4	200 W	Amorphous
5	400 W	Amorphous

peaks at 2θ of 6.05°, 10.02°, 11.7°, 15.4°, 20.1°, 23.3°, 26.7° and 30.9° belong to 111, 220, 311, 331, 511, 440, 533, and 642 planes of the Z-Y structure that corroborates the formation of Z-Y [30]. As seen, the structure of Z-Y without any impurities is formed after three hours.

FT-IR spectrum of the prepared Z-Y displays the strong peaks at 460, 567, and 1002 cm^{-1} that assigned to T-O (T = Si, Al) bending and Si-O, Al-O tetrahedral vibrations, respectively (Fig. 2) [31].

Fig. 3 (a, b) shows SEM images of the prepared Z-Y. As can be seen, the formation of hexagonal crystal shapes obtained after 3 h ultrasonic treatment. There are regular shapes that reveal a uniform particulate morphology with an average particle size of 80 nm.
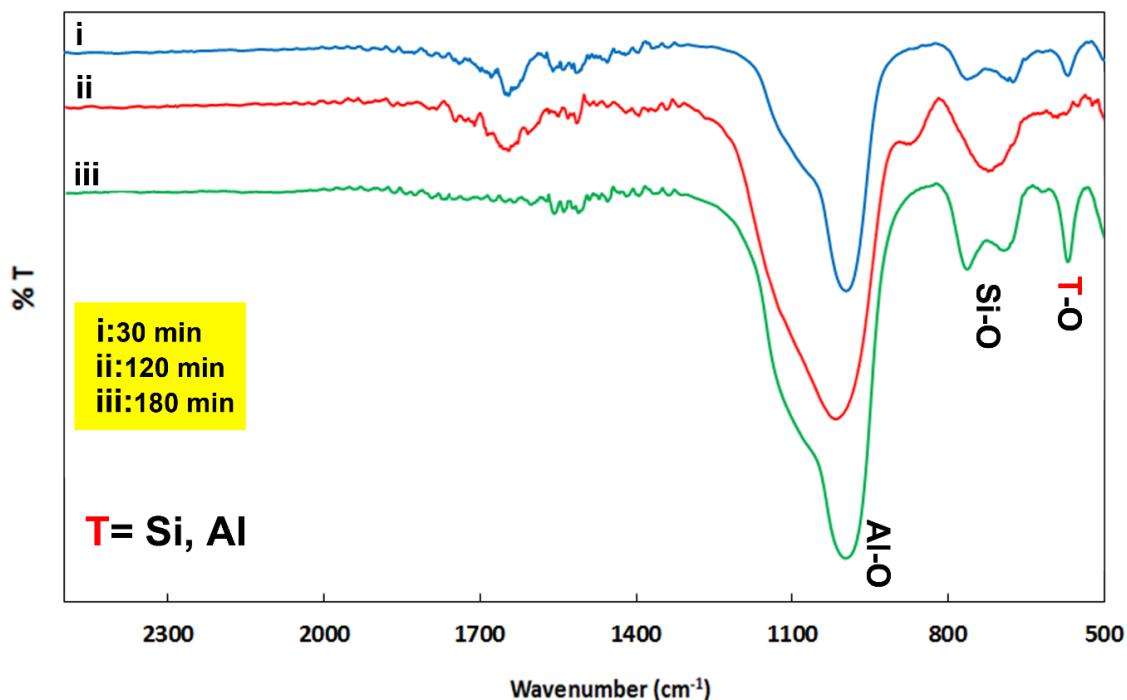

Fig. 2. FT-IR spectra for the synthesis of Z-Y in different times (30, 120, and 180 min).
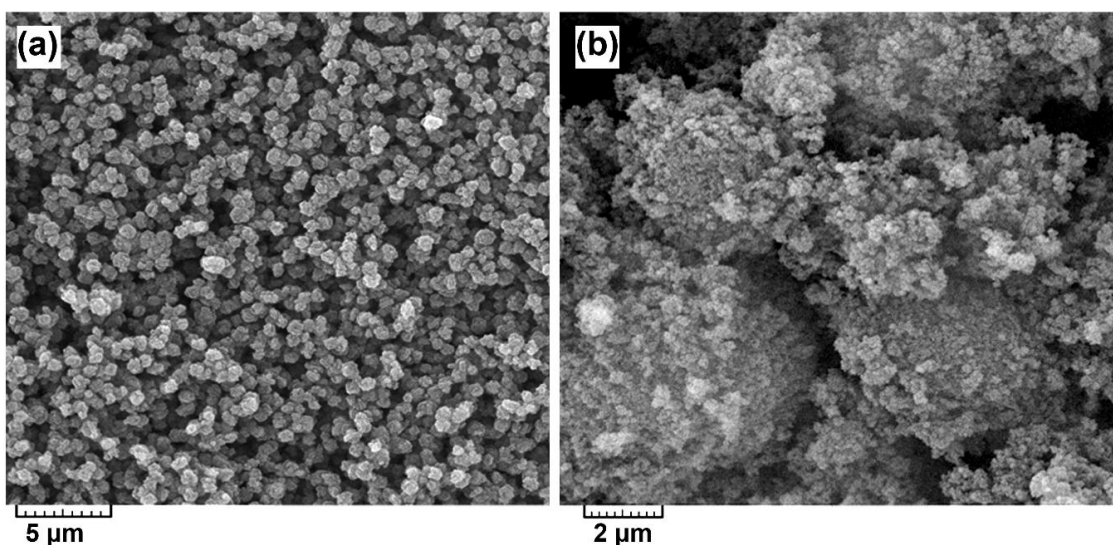

Fig. 3. SEM images (a, b) of the prepared Z-Y.

In this work, firstly Z-Y ion-exchanged to H-Y and then Z-Y-Pt NPs was synthesized. FT-IR spectrum of the prepared of Z-Y-Pt NPs is presented in Fig. 4. For the crystallization time after 1 h of ultrasonic treatment, the faujasite characteristic bands at 563, 712 and 1004 cm^{-1} appear, which could be associated with the double ring vibration and symmetric stretching vibration of the Al–O–Si in the zeolite framework, confirming that Z-Y crystals are formed [1].

Fig. 5 reveals the XRD pattern of the prepared Z-Y-Pt NPs. This prepared zeolite exhibits three diffraction peaks at 2θ = 40.03°, 46.9°, and 68.1 belong to 111, 200, and 220 planes of the Pt phase [32]. Also, sharp reflections at 2θ of 6.20°, 10.11°, 11.82°, 13.40°, 15.66°, 20.24°, 23.60°, 26.96°, and 31.2° belong to 111, 220, 311, 331, 511, 440, 533, 642, and 555 planes that confirm the Z-Y structure [31].

SEM and TEM images of the prepared Z-Y-Pt NPs are given in Fig. 6. It can be observed that this zeolite exhibited an important diminishing in its crystallinity compared to Z-Y (Fig. 6a). Because of time and temperature were less for the synthesis
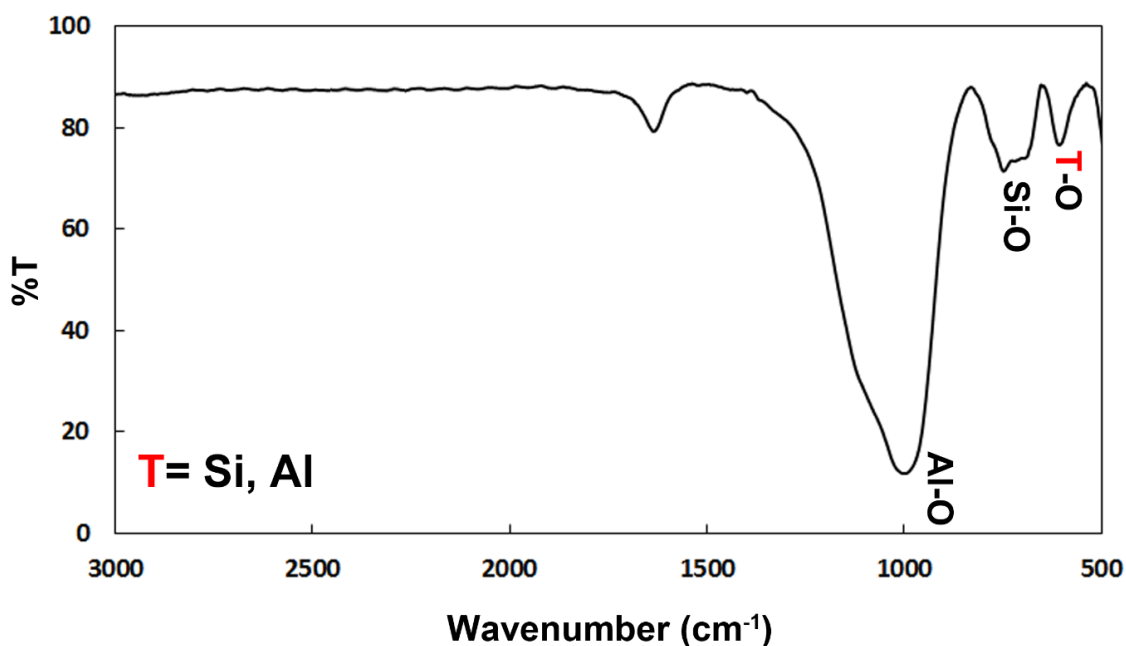

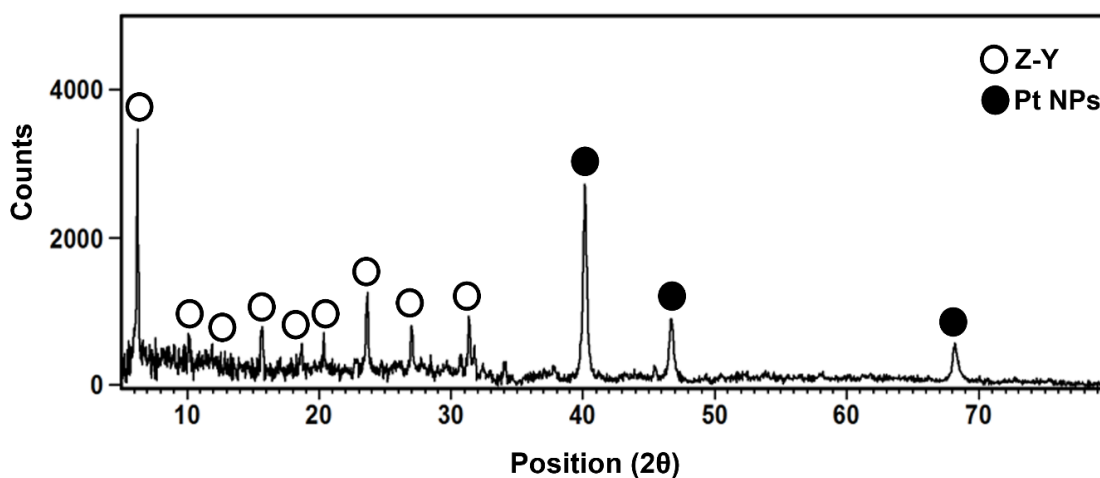Fig. 4. FT-IR spectrum of the prepared Z-Y-Pt NPs.

Fig. 5. XRD pattern of the prepared Z-Y-Pt NPs.

of Z-Y-Pt NPs in compared with Z-Y. This behavior is related to two main factors, 1) time of crystallization and 2) temperature for the synthesis. According to histogram size distribution of Z-Y-Pt NPs (Fig. 6c), the average diameter size of Z-Y is 0.17 µm. In the TEM image, Pt NPs appear as dark dots on a lighter shaded substrate corresponding to the Z-Y surface (Fig. 6b). The average diameter size of Pt NPs is 14.2 nm corresponding to histogram size distribution of Z-Y-Pt NPs (Fig. 6d). Also, the average crystallite size of the as prepared Pt NPs were calculated by the Scherer formula: $D = 0.9\lambda/(\beta \cos \theta)$, where D represents the crystallite size (nm), β is the full width of the diffraction line at half the maximum intensity, λ represents the wavelength of X-ray and θ is the Bragg angle [30]. The average crystallite size of about 8 nm obtained for the product using

XRD pattern and Debye–Scherrer equation. This value is lower than the obtained particle size of 14.2 nm resulted from TEM images for the Z-Y-Pt NPs. It returns to the difference of concept of the crystallite size and particle size. A particle may be made up of several different crystallites or just one crystallite that in this case is equal to particle size. We often report the particle size based on SEM and TEM images because we can't exactly determine whether the particle is one crystallite or composed of many compacted single crystals. The observed difference between the obtained values of XRD and TEM images can reveal that each particle of the product is a composed of small crystallites with the average crystallite size of about 8 nm.

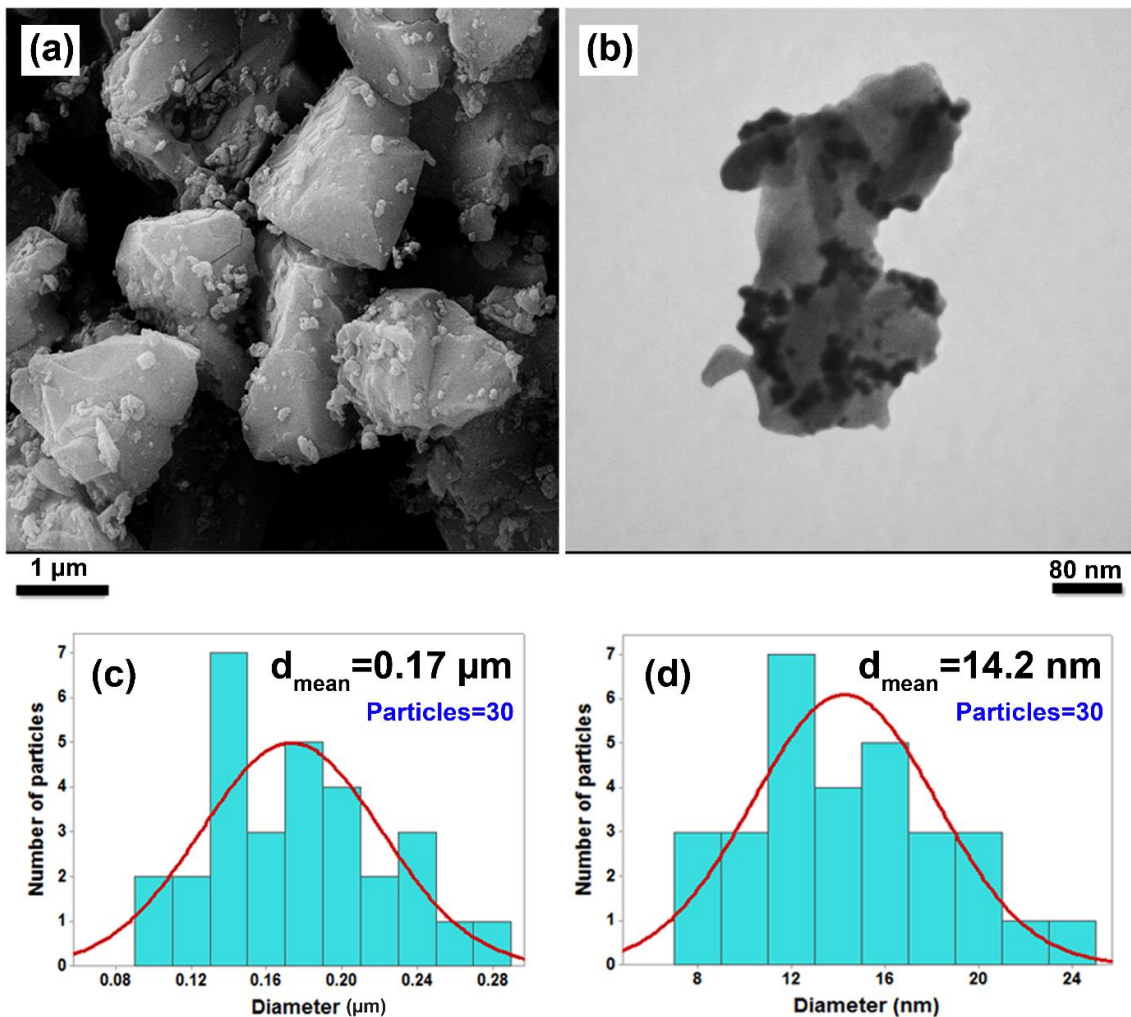Nitrogen adsorption–desorption

Fig. 6. a) SEM image of Z-Y-Pt NPs, b) TEM image of Z-Y-Pt NPs, c) histogram size distribution of Z-Y, and d) histogram size distribution of Pt NPs .
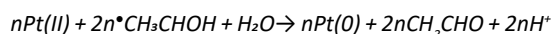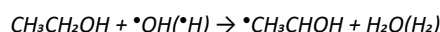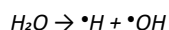
measurements were carried out at -196 °C on a Micromeritics ASAP 2020 instrument to determine the Brunauer Emmett Teller (BET) surface area of Z-Y and Z-Y-Pt NPs (Fig. 7a, 7c) and to estimate the mesopore size distribution using the Barrett Joyner Halenda (BJH) (Fig. 7b, 7d) calculation procedure. For these prepared zeolites, the isotherms display a hysteresis loop at a relative pressure of 0< P/P_0 <1, indicating a mesoporous structure for Z-Y and Z-Y-Pt NPs with BET surface area of 86.61 and 36 cm^2g^1, respectively (Fig. 7a and 7c). In addition, the mesopore diameters were obtained about 15.36 and 14.44 nm using BJH curves for Z-Y and Z-Y-Pt NPs, respectively (Fig. 7b and 7d). According to the results form BET and BJH curves, these prepared zeolites have good porous surfaces. Although, the BET surface area of Z-Y is reduced after reaction with H_2PtCl_6 and other ingredients in the reaction. Also, the placement of Pt NPs into zeolite cavities can be another reason for the reduction of pore volume.

Fig. 8 shows the chemical composition of the prepared Z-Y-Pt NPs and confirming the existence of Pt NPs (2.1 wt%) on the Z-Y body.

EDS mapping images were obtained from the synthesized Z-Y-Pt NPs (Fig. 9). According to this analyze, Pt NPs are homogenously distributed on the Z-Y surface. There is no coagulation in this prepared zeolite.

In this study, Pt NPs have been synthesized by the ultrasonic reduction method. After ultrasonic treatment, the reduction of Pt (II) ions could occur by generated organic radicals as the following reactions (1–3):

$$H_2O \rightarrow \bullet H + \bullet OH$$

$$CH_3CH_2OH + \bullet OH(\bullet H) \rightarrow \bullet CH_3CHOH + H_2O(H_2)$$

$$nPt(II) + 2n\bullet CH_3CHOH + H_2O \rightarrow nPt(0) + 2nCH_3CHO + 2nH^+$$

This proposed mechanism was reported by Okitsu [33].

A comparison of the prepared zeolite in this work and other zeolites has been given in Table 2. It shows that the synthesis of zeolites by hydrothermal method needs to consume the high energy and more time, whereas the synthesis of zeolites by ultrasonic method is performed in short time, low temperature or pressure. As can be seen, the prepared zeolite in this work needs very short time and low temperature.
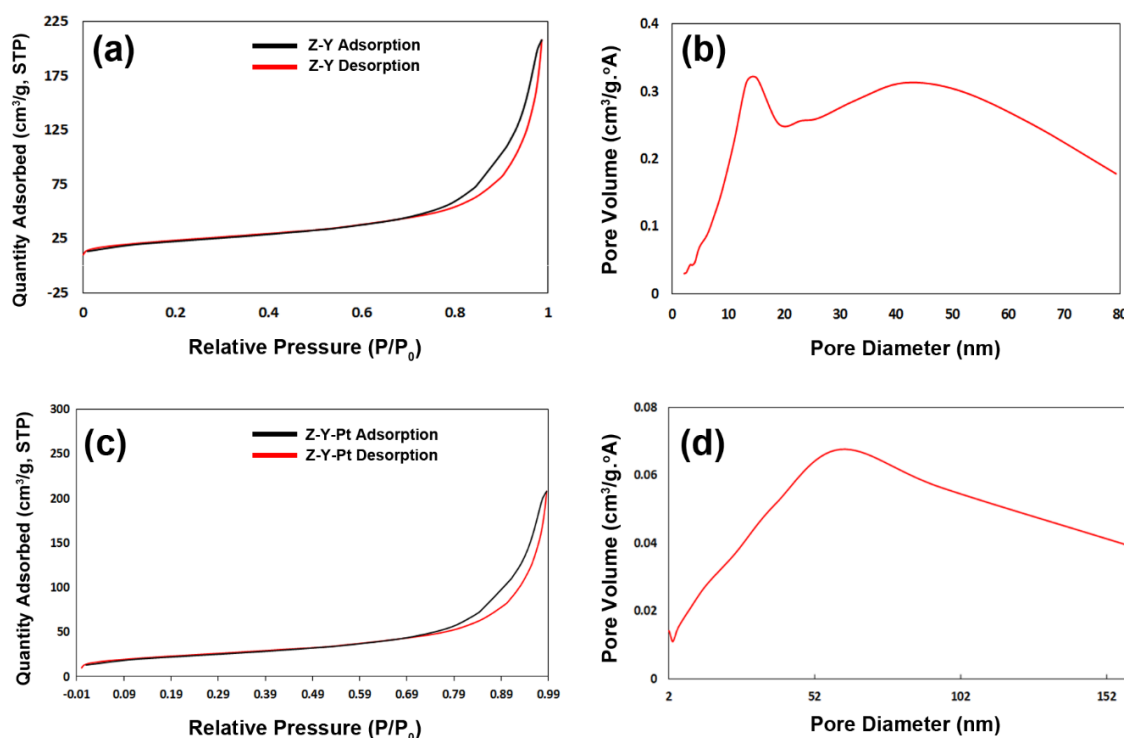

Fig. 7 a) BET analyze of Z-Y, b) BJH curve of Z-Y, c) BET analyze of Z-Y-Pt NPs and d) BJH curve of Z-Y-Pt NPs.
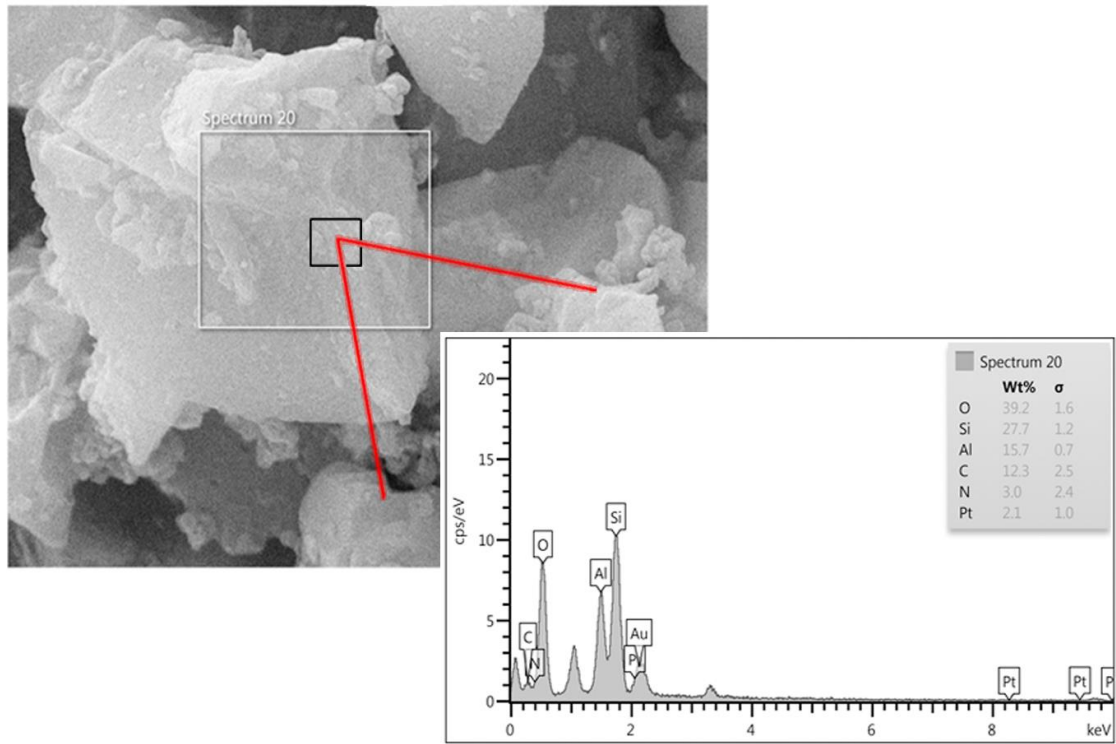
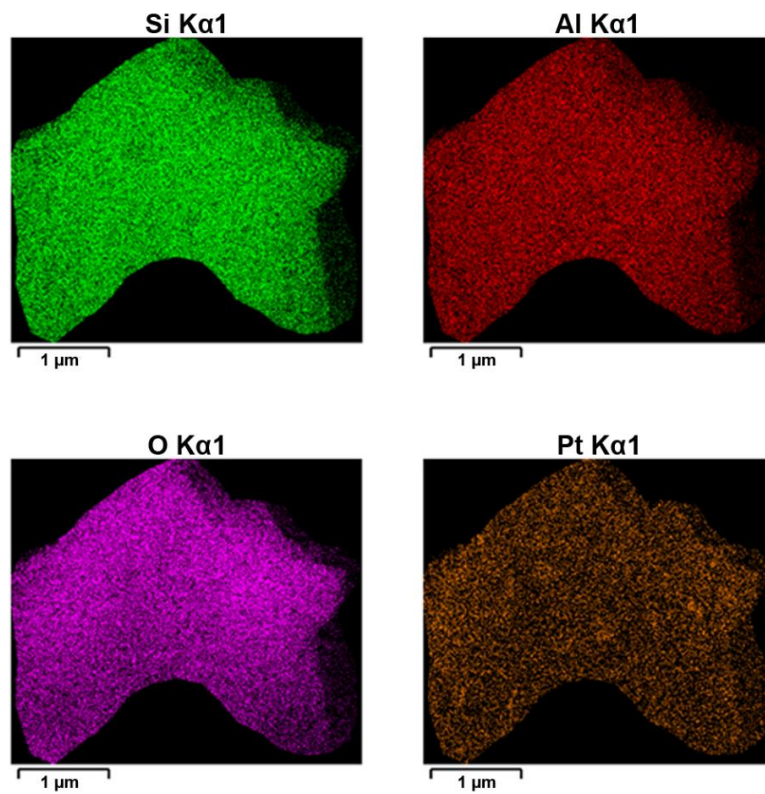Fig. 8. a) EDS analyze of the prepared Z-Y-Pt NPs.

Fig. 9. a) EDS mapping of the prepared Z-Y-Pt NPs.

Table 2. Synthesis different zeolites by hydrothermal and ultrasound methods.

Entry	Sample	Condition	Time (h)	Temperature (ºC)	Ref.
1	Pt@HBZ	Hydrothermal	10	140	[34]
2	Pt/4A-Z	Ultrasound	2.5	RT	[35]
3	Pt-H-ZSM-5	Ultrasound	3.0	RT	[36]
4	Pt@MFI	Hydrothermal	1.0	180	[37]
5	Pt/ZSM-5	Hydrothermal	12.0	100	[37]
6	Pt@IPC-2	Hydrothermal	16.0	170	[38]
7	Pt@IPC-4	Hydrothermal	16.0	140	[38]
8	Z-Y-Pt NPs	Ultrasound	1.0	RT	This work
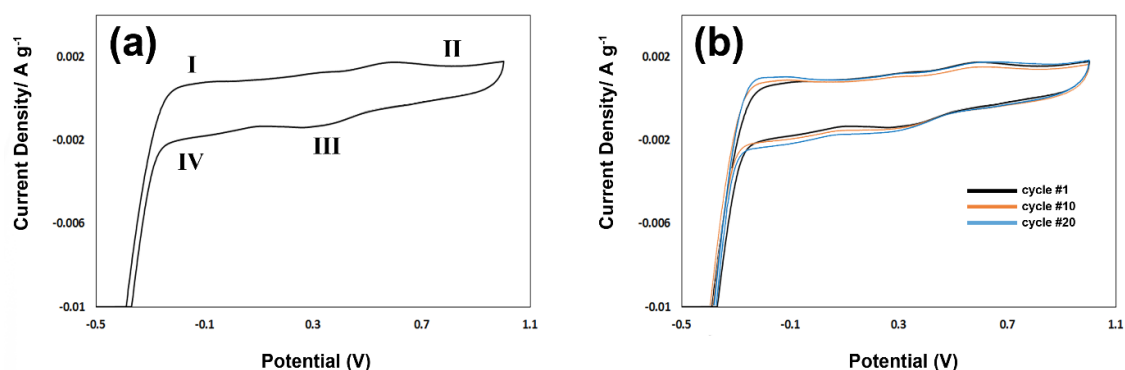
Fig. 10. CV curves of (a) the prepared Z-Y-Pt NPs and (b) at different cycles at the potential scan rate of 0.05 Vs^{-1}.

Investigation of the electrochemical characteristics of the prepared Z-Y-Pt NPs was carried out by the use of cyclic voltammetry (CV) test (Fig. 10a). The recorded CV of Z-Y-Pt NPs exhibited nearly rectangular curves of redox reaction pairs with humps during anodic scan. The humps on Z-Y-Pt NPs diagram are associated with atomic hydrogen desorption and adsorption (I and IV regions in Fig. 10a). Metal oxide formation and their reduction were also observed (II and III regions in Fig. 10a). If the maximum peak current density in the forward is designated as j_f and the maximum peak current density in the backward is designated as j_b, the ratio of j_f/j_b is generally used to evaluate the tolerance of the catalysts to incompletely oxidized species accumulated on the surface of the electrode. A larger ratio of j_f/j_b represents more complete oxidation, less accumulation of CO or CO-like species on the catalyst surface [39]. According to Fig. 10a, the j_f/j_b ratio for the synthesized Z-Y-Pt NPs is about 1.10. Also, study of the electrochemical properties revealed a capacity retention after 10 and 20 cycles with relatively overlapping of the CV cycles presenting a rather good cycling lifespan (Fig. 10b).

Due to the large use and applications of Pt metal and zeolite in chemistry, this sample can be applied for many applications such as industrial catalyst, adsorption, removing volatile organic colors and fuel cell. This work provide a short and facile method to obtain Pt NPs that supported on zeolite surface. Also, the size of the Pt NPs is small enough, which causes increasing its efficiency in chemical applications.

CONCLUSION

In this work, a simple and rapid method for the synthesis of Pt NPs supported on Z-Y surface is reported. Briefly, Z-Y was synthesized by the sonochemical method and then Pt NPs were deposited on the Z-Y surface using ultrasonic treatment at room temperature. The structure and morphology of the prepared Z-Y-Pt NPs were characterized using FT-IR, XRD, SEM, TEM, EDS, EDS mapping, and BET analysis. According to the results, this prepared zeolite has uniform particulate morphology with a good surface area. Also, Pt NPs with diameter size of 14 nm, are homogenously distributed on the Z-Y surface. Compared to other methods for the synthesis of Pt NPs on the zeolite surface, this method needs very short time and low temperature. Also, using

ultrasonic is a green and Eco-friendly method for the synthesis of compounds in chemistry that is attracted a lot of attention in recent years. The prepared Z-Y-Pt NPs in this work has been applied in CV test for investigation of its activity. Our study shows that the synthesized Z-Y-Pt NPs has good activity toward CV test and it displays ratio of j_f/j_b =1.10 that can be suitable for redox reaction in fuel cell.

ACKNOWLEDGMENT

CONFLICT OF INTEREST

The authors declare that there are no conflicts of interest regarding the publication of this manuscript.

REFERENCES

1. Tang T, Zhang L, Dong H, Fang Z, Fu W, Yu Q, et al. Organic template-free synthesis of zeolite Y nanoparticle assemblies and their application in the catalysis of the Ritter reaction. RSC Advances. 2017;7(13):7711-7717.

2. Bacakova L, Vandrovcova M, Kopova I, Jirka I. Applications of zeolites in biotechnology and medicine – a review. Biomaterials Science. 2018;6(5):974-989.

3. Li Y, Liu S, Zhang Z, Xie S, Zhu X, Xu L. Aromatization and isomerization of 1-hexene over alkali-treated HZSM-5 zeolites: Improved reaction stability. Applied Catalysis A: General. 2008;338(1-2):100-113.

4. Srivastava R, Choi M, Ryoo R. Mesoporous materials with zeolite framework: remarkable effect of the hierarchical structure for retardation of catalyst deactivation. Chem Commun. 2006(43):4489.

5. Kox MHF, Stavitski E, Groen JC, Pérez-Ramírez J, Kapteijn F, Weckhuysen BM. Visualizing the Crystal Structure and Locating the Catalytic Activity of Micro- and Mesoporous ZSM-5 Zeolite Crystals by Using In Situ Optical and Fluorescence Microscopy. Chemistry - A European Journal. 2008;14(6):1718-1725.

6. PÃ©rez-RamÃrez J, Verboekend D, Bonilla A, AbellÃ³ Sn. Zeolite Catalysts with Tunable Hierarchy Factor by Pore-Growth Moderators. Adv Funct Mater. 2009;19(24):3972-3979.

7. Sadeghbeigi R. Chemistry of FCC Reactions. Fluid Catalytic Cracking Handbook: Elsevier; 2012. p. 125-135.

8. Pérez-Ramírez J, Abelló S, Bonilla A, Groen JC. Tailored Mesoporosity Development in Zeolite Crystals by Partial Detemplation and Desilication. Adv Funct Mater. 2009;19(1):164-172.

9. Bjørgen M, Joensen F, Spangsberg Holm M, Olsbye U, Lillerud K-P, Svelle S. Methanol to gasoline over zeolite H-ZSM-5: Improved catalyst performance by treatment with NaOH. Applied Catalysis A: General. 2008;345(1):43-50.

10. Qin Z, Shen B, Gao X, Lin F, Wang B, Xu C. Mesoporous Y zeolite with homogeneous aluminum distribution obtained by sequential desilication–dealumination and its performance in the catalytic cracking of cumene and 1,3,5-triisopropylbenzene. J Catal. 2011;278(2):266-275.

11. M. Sadeghi; M. H. Hosseini, Preparation and Application of MnO_2 Nanoparticles/Zeolite AgY Composite Catalyst by Confined Space Synthesis (CSS) Method for the Desulfurization and Elimination of SP and OPP. J Nanostruct., 2012; (2): 441-455..

12. Wang B, Lin M, Peng X, Zhu B, Shu X. Hierarchical TS-1 synthesized effectively by post-modification with TPAOH and ammonium hydroxide. RSC Advances. 2016;6(51):44963-44971.

13. Chen F, Cao Q, Dong C, Shao B, Zhai W, Ma X, et al. Ultrasonic polymerization of CuO@PNIPAM and its temperature tuning glucose sensing behavior. Ultrason Sonochem. 2018;49:190-195.

14. Gordina NE, Prokof'ev VY, Kul'pina YN, Petuhova NV, Gazahova SI, Hmylova OE. Effect of ultrasound on the synthesis of low-modulus zeolites from a metakaolin. Ultrason Sonochem. 2016;33:210-219.

15. Vaičiukynienė D, Kantautas A, Vaitkevičius V, Jakevičius L, Rudžionis Ž, Paškevičius M. Effects of ultrasonic treatment on zeolite NaA synthesized from by-product silica. Ultrason Sonochem. 2015;27:515-521.

16. Monsef R, Ghiyasiyan-Arani M, Salavati-Niasari M. Application of ultrasound-aided method for the synthesis of $NdVO_4$ nano-photocatalyst and investigation of eliminate dye in contaminant water. Ultrason Sonochem. 2018;42:201-211.

17. Belviso C, Cavalcante F, Lettino A, Fiore S. Effects of ultrasonic treatment on zeolite synthesized from coal fly ash. Ultrason Sonochem. 2011;18(2):661-668.

18. Abrishamkar M, Azizi Seyed N, Kazemian H. Ultrasonic-Assistance and Aging Time Effects on the Zeolitation Process of BZSM-5 Zeolite. Z Anorg Allg Chem. 2010;636(15):2686-2690.

19. Azizi Seyed N, Yousefpour M. Static and Ultrasonic-assisted Aging Effects on the Synthesis of Analcime Zeolite. Z Anorg Allg Chem. 2010;636(5):886-890.

20. Andaç Ö, Tatlıer M, Sirkecioğlu A, Ece I, Erdem-Şenatalar A. Effects of ultrasound on zeolite A synthesis. Microporous Mesoporous Mater. 2005;79(1-3):225-233.

21. Herrmann R, Schwieger W, Scharf O, Stenzel C, Toufar H, Schmachtl M, et al. In situ diagnostics of zeolite crystallization by ultrasonic monitoring. Microporous Mesoporous Mater. 2005;80(1-3):1-9.

22. Musyoka NM, Petrik LF, Hums E, Baser H, Schwieger W. In situ ultrasonic diagnostic of zeolite X crystallization with novel (hierarchical) morphology from coal fly ash. Ultrasonics. 2014;54(2):537-543.

23. Belviso C, Lettino A, Cavalcante F. Influence of Synthesis Method on LTA Time-Dependent Stability. Molecules. 2018;23(9):2122.

24. Wang B, Wu J, Yuan Z-Y, Li N, Xiang S. Synthesis of MCM-22 zeolite by an ultrasonic-assisted aging procedure. Ultrason Sonochem. 2008;15(4):334-338.

25. Ghiyasiyan-Arani M, Salavati-Niasari M. Effect of $Li_2CoMn_3O_8$ Nanostructures Synthesized by a Combustion Method on Montmorillonite K10 as a

Potential Hydrogen Storage Material. The Journal of Physical Chemistry C. 2018;122(29):16498-16509.

26. Mazloom F, Ghiyasiyan-Arani M, Monsef R, Salavati-Niasari M. Photocatalytic degradation of diverse organic dyes by sol–gel synthesized $Cd_2V_2O_7$ nanostructures. Journal of Materials Science: Materials in Electronics. 2018;29(21):18120-18127.

27. Razavi FS, Morassaei MS, Salehabadi A, Ghiyasiyan-Arani M, Salavati-Niasari M. Structural characterization and electrochemical hydrogen sorption performances of the polycrystalline $Ba_2Co_9O_{14}$ nanostructures. J Alloys Compd. 2019;777:252-258.

28. Monsef R, Ghiyasiyan-Arani M, Salavati-Niasari M. Utilizing of neodymium vanadate nanoparticles as an efficient catalyst to boost the photocatalytic water purification. J Environ Manage. 2019;230:266-281.

29. Hoseini SJ, Bahrami M, Dehghani M. Formation of snowman-like Pt/Pd thin film and Pt/Pd/reduced-graphene oxide thin film at liquid–liquid interface by use of organometallic complexes, suitable for methanol fuel cells. RSC Advances. 2014;4(27):13796.

30. Tadjarodi A, Dehghani M, Imani M. Green synthesis and characterization of palladium nanoparticles supported on zeolite Y by sonochemical method, powerful and efficient catalyst for Suzuki-Miyaura coupling of aryl halides with phenylboronic acid. Appl Organomet Chem. 2018;32(12):e4594.

31. Dehghani M, Tadjarodi A, Chamani S. Synthesis and Characterization of Magnetic Zeolite Y–Palladium–Nickel Ferrite by Ultrasonic Irradiation and Investigating Its Catalytic Activity in Suzuki–Miyaura Cross-Coupling Reactions. ACS Omega. 2019;4(6):10640-10648.

32. Hoseini SJ, Bahrami M, Sadri N, Aramesh N, Fard ZS, Iran HR, et al. Multi-metal nanomaterials obtained from oil/water interface as effective catalysts in reduction of 4-nitrophenol. J Colloid Interface Sci. 2018;513:602-616.

33. Okitsu K, Bandow H, Maeda Y, Nagata Y. Sonochemical Preparation of Ultrafine Palladium Particles. Chem Mater. 1996;8(2):315-317.

34. Dai R, Zheng Z, Sun C, Li X, Wang S, Wu X, et al. Pt nanoparticles encapsulated in a hollow zeolite microreactor as a highly active and stable catalyst for low-temperature ethanol steam reforming. Fuel. 2018;214:88-97.

35. Cai N, Wu J, Jin C. 4A Zeolite Support for Pt Nanoparticles towards Methanol Oxidation. J Electrochem Soc. 2019;166(10):H387-H391.

36. Sápi A, Kashaboina U, Ábrahámné KB, Gómez-Pérez JF, Szenti I, Halasi G, et al. Synergetic of Pt Nanoparticles and H-ZSM-5 Zeolites for Efficient CO_2 Activation: Role of Interfacial Sites in High Activity. Frontiers in Materials. 2019;6.

37. Gu J, Zhang Z, Hu P, Ding L, Xue N, Peng L, et al. Platinum Nanoparticles Encapsulated in MFI Zeolite Crystals by a Two-Step Dry Gel Conversion Method as a Highly Selective Hydrogenation Catalyst. ACS Catalysis. 2015;5(11):6893-6901.

38. Zhang Y, Kubů M, Mazur M, Čejka J. Encapsulation of Pt nanoparticles into IPC-2 and IPC-4 zeolites using the ADOR approach. Microporous Mesoporous Mater. 2019;279:364-370.

39. Hsin YL, Hwang KC, Yeh C-T. Poly(vinylpyrrolidone)-Modified Graphite Carbon Nanofibers as Promising Supports for PtRu Catalysts in Direct Methanol Fuel Cells. J Am Chem Soc. 2007;129(32):9999-10010.